RSC Advances

PAPER

View Article Online
View Journal | View Issue

Cite this: *RSC Adv.*, 2016, **6**, 108328

Two new silver triazole frameworks with polyoxometalate templates†

Jingquan Sha,*[a] Xiya Yang,[a] Peipei Zhu,[a] Yaqian Lan*[b] and Ning Sheng[a]

Received 25th September 2016
Accepted 28th October 2016

DOI: 10.1039/c6ra23809b

www.rsc.org/advances

Two new polyoxometalate-templated organic–inorganic hybrid compounds with different metal–organic frameworks, $[Ag_5(trz)_6][H_4PMo_{12}O_{40}]$ (**1**) and $[Ag_{10}(trz)_8][HPMo_{12}O_{40}]$ (**2**) (trz = 1,2,4-triazole), have been prepared based on the same organic ligands under different pH values. Compound **1** exhibits a honeycomb 2D $[Ag_5(trz)_6]$ network and 3D graphite-like hybrid framework, and compound **2** exhibits a 3D $\{Ag_3[Ag_6(trz)_6][Ag(trz)_2]\}$ framework with 2D channels, in which $[PMo_{12}O_{40}]^{3-}$ polyanions locate in the center of channels. To the best of our knowledge, $[PMo_{12}O_{40}]^{3-}$ polyanions represent the highest coordination number in **1** and terminal oxygen coordination number in **2** of Keggin POMs up to date. A comparison of two compounds demonstrates that the coordination mode of 1,2,4-triazole ligands and Keggin POMs templates have important influences on the assembly of different frameworks. In addition, compounds **1** and **2** exhibit good photocatalytic degradation of Rhodamine-B, and are very stable and easily recyclable as well.

Introduction

New porous materials such as zeolites and zeolite-like compounds have aroused increasing interest owing to their potential applications in gas storage,[1,2] ion exchange,[3,4] selective catalysis,[5,6] molecular sieves,[7,8] and so on.[9] In this field, the use of templates such as organic amine cations[10,11] and some small anions[12,13] (Cl^-, Br^-, I^-, ClO_4^- and PF_6^-), is a current important synthetic strategy. In addition, large inorganic anions can also be employed as templates to construct new porous compounds.[14,15] Polyoxometalates (POMs), one kind of significant inorganic anions with versatile structural topologies and abundant chemical combinations,[16–18] could exert the template role to direct the construction of new cationic metal–organic frameworks (MOFs). For example, Zubieta reported the first 3D tpypor based cationic framework $[Fe_4(tpypor)_3]_n^{4n+}$ (tpypor = tetrapyridylporphyrin) with $\{Mo_6O_{19}\}$ template.[19] Lu and co-workers synthesized the first 3D [6]catenane framework [Agtrz] $[Ag_{12}trz_9][PMo_{12}O_{40}]$ in 2010 and the pseudorotaxane framework $Ag_{14}(trz)_{10}[SiW_{12}O_{40}]$ in 2011 with Keggin POMs template (trz = 1,2,4-triazole).[20,21] Moreover POMs as templates can be incorporated into some special structural frameworks, such as POM@MIL-101,[22,23] POM@HKUST-1,[24,25] and POM@rht-MOF-1.[26]

As is known to all that surface oxygen atoms of POMs are rather reactive and easily incorporate with the highly oxophilic metal ions.[27–29] What's more vital, the resulting POMs–metal subunits can provide considerable metal atoms for directing the fabrication of novel framework.[30,31] However, to a large number of surface oxygen atoms (36 and 54 for Keggin POMs and Wells-Dawson POMs, respectively), the highest coordination numbers are not more than 9 for Keggin POMs[32] and 16 for Wells-Dawson POMs[33] to date. Therefore, there is more space to extend the structural multiformity in face of the rich coordination oxygen atoms of POMs. At present, organonitrogen ligands have become the preferred choice to assemble POM-based hybrid compounds,[34,35] in particular, the small-size triazole molecules such as 1,2,3-triazole[36] and 1,2,4-triazole,[37] because triazole molecules unite the coordination modes of both pyrazole and imidazole, which exhibits the extensively coordination ability to bridge metal ions with unusual structural diversity.[38] Hence, triazole molecules were fully considered in our synthetic efforts for new POM-templated hybrid framework. In this work, two new Ag–trz frameworks with Keggin POMs templates, $[Ag_5(trz)_6][H_4PMo_{12}O_{40}]$ (**1**) and $[Ag_{10}(trz)_8][HPMo_{12}O_{40}]$ (**2**), (trz = 1,2,4-triazole) were obtained under different pH values by hydrothermal reaction. In addition, the formation of Ag–trz frameworks with Keggin POMs template is discussed and the catalytical activities using the photocatalytic degradation of Rhodamine-B as model are also reported.

[a]*Key Laboratory of Inorganic Chemistry in Universities of Shandong, Department of Chemistry and Chemical Engineering, Jining University, Qufu, 273155, China. E-mail: shajq2002@126.com*

[b]*Jiangsu Key Laboratory of Biofunctional Materials, College of Chemistry and Materials Science, Nanjing Normal University, Nanjing 210023, P. R. China. E-mail: yqlan@njnu.edu.cn*

† Electronic supplementary information (ESI) available: Tables of selected bond lengths (Å), bond angles (deg) and IR and XRPD and structural figures for compounds **1** and **2**. CCDC 1494914 and 1494913 contains the supplementary crystallographic data for compounds **1** and **2**, respectively. For ESI and crystallographic data in CIF or other electronic format see DOI: 10.1039/c6ra23809b

Experimental materials and general methods

All reagents were reagent grade and used as purchased commercially without further purification. All syntheses were carried out in 20 mL polytetrafluoroethylene lined stainless steel containers under autogenous pressure. Elemental analyses for C, H, N were performed on a Perkin-Elmer 2400 CHN Elemental Analyzer. The IR spectrum was obtained on an Alpha Centaurt FT/IR spectrometer with KBr pellet in the 400–4000 cm^{-1} region. The XRPD patterns were obtained with a Rigaku D/max 2500 V PC diffractometer with Cu-Kα radiation, the scanning rate is 4° s^{-1}, 2θ ranging from 5–40°. UV-vis absorption spectra were recorded on a 756 CRT UV-vis spectrophotometer.

Synthesis of $[Ag_5(trz)_6][H_4PMo_{12}O_{40}]$ (1)

$H_3PMo_{12}O_{40}$ (300 mg, 0.16 mmol), $AgNO_3$ (150 mg, 0.89 mmol), trz (50 mg, 0.72 mmol), NH_4VO_3 (36 mg, 0.31 mmol) were dissolved in distilled water (10 mL) with stirring for 0.5 h at room temperature, and pH value was adjusted to *ca.* 3.0 by 1 mol L^{-1} HCL. The resulting solution was transferred into the 20 mL polytetrafluoroethylene lined stainless steel reactor and heated at 170 °C for 5 days. After the autoclave was cooled to room temperature at 10 °C h^{-1}, the yellow block crystal suitable for X-ray crystallography were obtained, and then washed with distilled water and air-dried (yield: 35% based on Ag). Elemental analysis: anal. calcd for $Ag_5C_{12}N_{18}H_{16}Mo_{12}O_{40}P$ (2774.00): calcd C 5.19, H 0.58, N 9.08%; found C 5.17, H 0.64, N 9.06%.

Table 1 Crystal data and structure refinements for the compounds **1** and **2**[a]

Chemical formula	$C_{12}N_{18}H_{16}Ag_5PMo_{12}O_{40}$	$C_{16}N_{24}H_{16}Ag_{10}PMo_{12}O_{40}$
Formula weight	2774	3446.38
CCDC	1494914	1494913
Temperature (K)	273	298
Wavelength (Å)	71.073	71.073
Crystal system	Trigonal	Triclinic
Space group	$P\bar{3}1m$	$P\bar{1}$
a (Å)	12.1615	11.0695
b (Å)	12.1615	12.3229
c (Å)	10.4558	13.1699
α (°)	90	79.160
β (°)	90	66.215
γ (°)	120	72.255
V (Å^3)/Z	1339.25/1	1561.31/1
Density (g cm^{-3})	3.435	3.664
Abs coeff. (mm^{-1})	4.630	5.507
F(000)	1284.0	1589.0
Data collect θ range	3.350 to 29.282°	3.303 to 29.312°
Reflns collected	10 628	20 476
Independent reflns	1262	7404
R_{int}	0.0410	0.0307
Data/restraints/parameters	1262/123/109	7404/0/482
Goodness-of-fit on F^2	1.023	1.047
Final R indices [$I > 2\delta(I)$]	$R_1 = 0.0534$, wR_2 = 0.1224	$R_1 = 0.0493$, wR_2 = 0.0974
R Indices (all data)	$R_1 = 0.0670$, wR_2 = 0.1293	$R_1 = 0.0653$, wR_2 = 0.1036
Largest diff. peak and hole (e Å^{-3})	1.087 and −1.276	1.282 and −1.267

[a] $R_1 = \Sigma(||F_o| - |F_c||)/\Sigma|F_o|$, $wR_2 = \Sigma w(|F_o|^2 - |F_c|^2)^2/\Sigma w(|F_o|^2)^2]^{1/2}$.

Synthesis of $[Ag_{10}(trz)_8][HPMo_{12}O_{40}]$ (2)

The synthetic method was similar to that of compound **1**, except that pH value was adjusted to *ca.* 4.5 with 1 M KOH. Red block crystals of **2** were filtered, washed with water, and dried at room temperature (26% yield based on Ag). Elemental analysis: anal. calcd for $Ag_{10}C_{16}N_{24}H_{17}Mo_{12}O_{40}P$, (3446.38): calcd. C 5.58, H 0.49, N 9.75%; found C 5.57, H 0.55, N 9.72%.

X-ray crystallographic study

Crystallographic data for compounds **1** and **2** were collected on the Agilent Technology Eos Dual system with Mo-Kα radiation (λ = 0.71069 Å) at 293 K. The structures were solved by the direct method and refined full-matrix last squares on F^2 through the SHELXTL and WINGX software package.[39] All non-hydrogen atoms were refined anisotropically and the ISOR command was used to refine some APD and NPD atoms in **1** and **2**. The crystal data and selected bond lengths and angles are listed in Tables 1, S1 and S2.† CCDC reference numbers 1494914 for **1** and 1494913 for **2**.

Photocatalysis properties

To investigate the photocatalytic activities of compounds **1** and **2** as catalyst, the photodecomposition of Rhodamine-B (RhB) is evaluated under UV light irradiation through a typical process: **1** or **2** (50 mg) was mixed together with 100 mL of 1.0×10^{-5} mol L^{-1} (C_0) RhB solution in a beaker by ultrasonic dispersion for 10 min. The mixture was stirred for *ca.* 30 min till reached the surface-adsorption equilibrium on the particles of compounds. Then the mixture was stirred continuously under ultraviolet (UV) irradiation from a 125 W high pressure Hg lamp. At 0, 20, 40, 60, 90, 120 and 150 min, 3 mL of the sample was taken out from the beaker respectively, followed by several centrifugations to remove the title compound and a clear solution was obtained for UV-vis analysis.

Results and discussion

Single-crystal X-ray diffraction analysis shows that compound **1** crystallizes in the trigonal space group $P\bar{3}1m$ and shows a 3D framework constructed by 2D $[Ag_5(trz)_6]$ net and 1D POM–Ag inorganic chains. Compound **2** crystallizes in the triclinic space group $P\bar{1}$ and exhibits a 3D framework constructed by 3D $\{Ag_3[Ag_6(trz)_6][Ag(trz)_2]\}$ framework and 2D POM–Ag inorganic layer. All Mo atoms are in +VI oxidation state in **1** and **2**, which was confirmed by valence sum calculations.[40] To balance the charge, some proton are added into the PMo_{12} polyanion, and compounds are formulated as $[Ag_5(trz)_6][H_4PMo_{12}O_{40}]$ (**1**) and $\{Ag_3[Ag(trz)_2][Ag_6(trz)_6]\}[HPMo_{12}O_{40}]$ (**2**). The networks of compounds were analyzed by using the TOPOS40 program.[41]

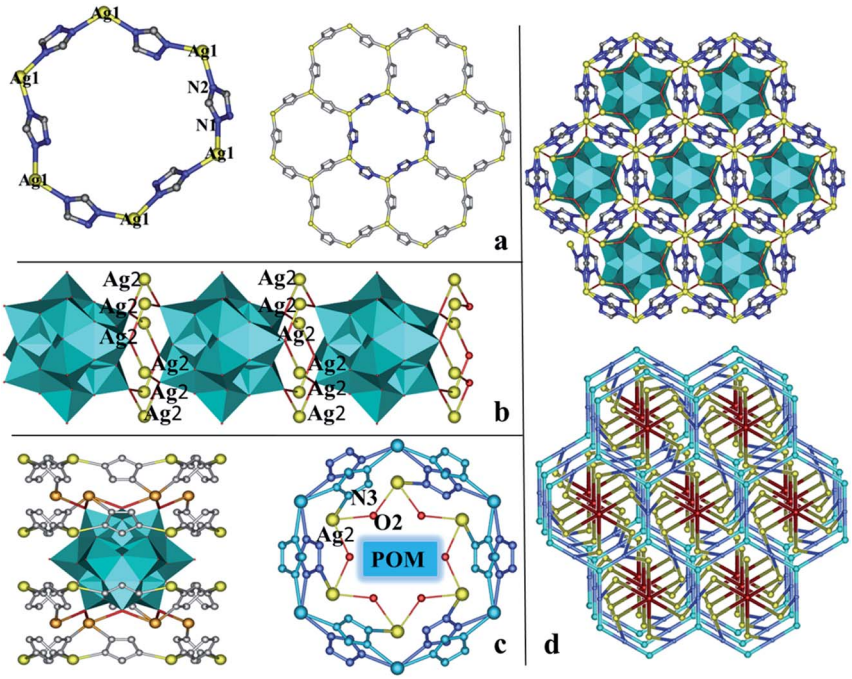

Fig. 1 (a) Ball/stick representation of the $[Ag_6(trz)_6]$ metallacycles and the 2D $[Ag_2(trz)_3]_n$ net of compound **1**. Only parts of atoms are labeled, and all hydrogen atoms are omitted for clarity. (b) Combined ball and polyhedral representations of the 1D POM–Ag inorganic chains. (c) Combined ball/stick and polyhedral representation of the connection mode of PMo_{12} clusters and metal–organic sheets. (d) Combined ball/stick and polyhedral and topology representation of the whole 3D structure constructed by PMo_{12} clusters (red), Ag1 (blue) Ag2 (yellow), trz ligand (blue).

The parallel experiments indicate that the use of NH_4VO_3 species is necessary and pH value plays a key role during the formation of compounds **1** and **2**.

Structure description of compound 1

Single crystal X-ray diffraction analysis reveals that **1** consists of five Ag^+ ions, six trz molecules and one $[PMo_{12}O_{40}]^{3-}$ polyanion (abbreviate as PMo_{12}) in Fig. S1 (ESI†). There are one crystallographically independent PMo_{12} polyanion and one disorder trz molecule, and two crystallography independent Ag ions (Ag1 and Ag2). And their coordination modes are illustrated in Fig. S2 (ESI†). The bond lengths around Ag ions are in range of 2.260–2.761 Å for Ag–N bond and 2.931 Å for Ag–O bond, while the N–Ag–N angles are in the range of 117.5–166.5°. Without regard to the PMo_{12} polyanions, Ag ions and trz molecules fabricate the 2D honeycomb network $[Ag_2(trz)_3]_n$ composed of the hexanuclear $[Ag_6(trz)_6]$ metallacycles with the dimensions of 14 Å × 12 Å, in which each Ag1 ions adopts triangular coordination mode completed by three N atoms from three trz molecules (Fig. 1a). In turn, taking no account of organic ligands, the PMo_{12} polyanions link with twelve Ag2 ions forming the 1D inorganic chain (Fig. 1b). To the best of our knowledge, the coordination number of PMo_{12} polyanions in **1** represents the highest coordination number of Keggin POMs up to date. As a whole, the POM–Ag2 chains and 2D $[Ag_2(trz)_3]_n$ network fuse together fabricating 3D framework with graphite-like structure *via* Ag2–N3 bonds (Fig. 1c and d), in which PMo_{12} polyanions are sandwiched between the center of networks. From the topological view, compound **1** exhibits an unique (3, 3, 3, 12)-connected 3D framework with an unprecedented $\{8^3\}\{4.8^2\}\{8^3\}\{4^{30}\cdot12^{30}\cdot14^6\}$ topology (Fig. 3d). In this simplification, the 3-connected nodes are Ag1, Ag2 ions and trz liginds, and the 12-connected nodes are PMo_{12} polyanions.

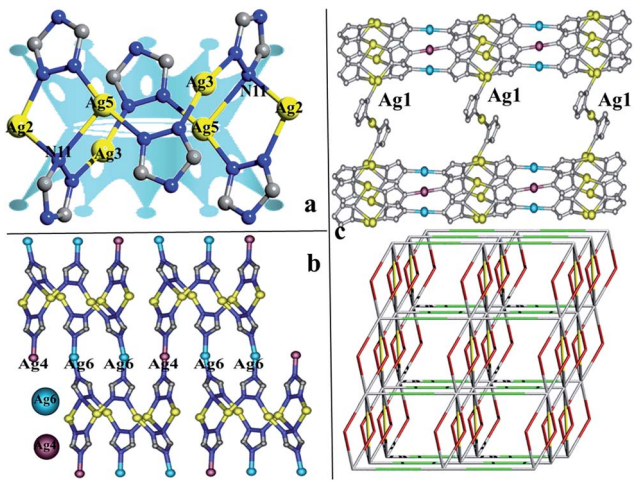

Fig. 2 (a) Ball/stick representation of the $[Ag_6(trz)_6]$ metallacycles of compound **2**. Only parts of atoms are labeled, and all hydrogen atoms are omitted for clarity. (b) Ball/stick representation representations of the 2D metal–organic sheet. (c) Combined ball/stick and topology representation of the whole 3D metal–organic framework with the larger void (*ca.* 22.242 Å × 22.242 Å).

Structure description of compound 2

Single crystal X-ray diffraction analysis reveals that compound **2** consists of ten Ag^+ ions, eight trz molecules and one

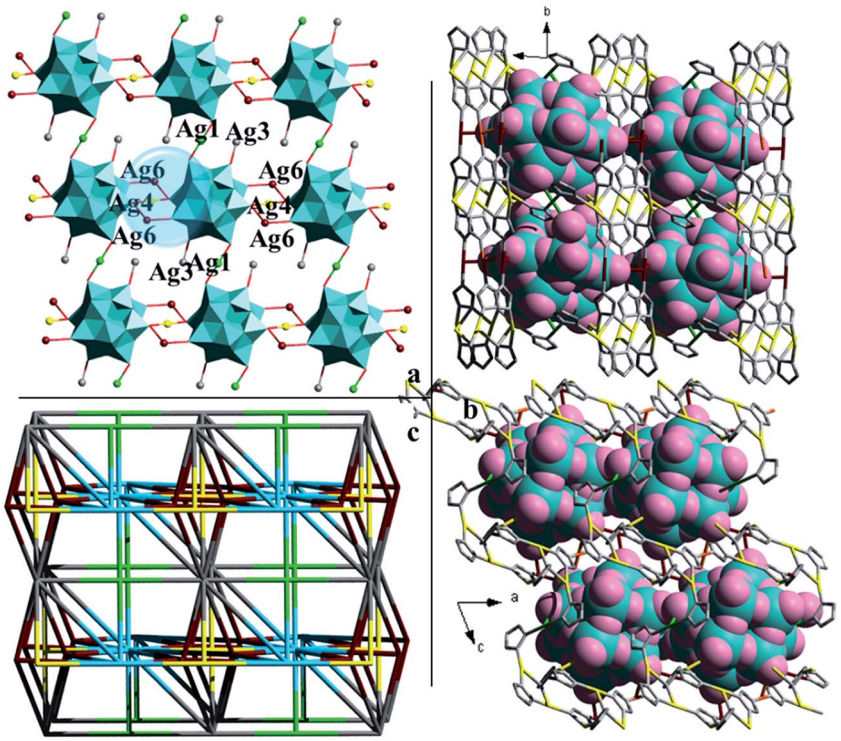

Fig. 3 (a) Combined ball/stick and polyhedral representations of the 2D POM–Ag inorganic layer constructed by the PMo_{12} clusters and Ag ions. (b) Combined space-filling and stick representation of the whole 3D structure in different orientation. (c) Topological representation of the whole 3D framework constructed by PMo_{12} clusters (bule), $[Ag_6(trz)_6]$ metallacycles (gray), Ag1 (green) Ag4 (yellow), Ag6 (dull red).

$[PMo_{12}O_{40}]^{3-}$ polyanion (abbreviate as PMo_{12}) as shown in Fig. S3 (ESI†). There are six crystallography independent Ag ions (Ag1, Ag2, Ag3, Ag4, Ag5, Ag6) and four crystallography independent trz ligands (trz-1, trz-2, trz-3, trz-4), and their coordination modes are illustrated in Fig. S4.† The bond lengths around Ag ions are in range of 2.72–2.86 Å for Ag–O bond, and 2.11–2.62 Å for Ag–N bond, while the N–Ag–N angles are in the range of 92.4–180.0°. Without regard to the PMo_{12} clusters, Ag ions and trz ligands fabricate a new 3D $\{Ag_3[Ag_6(trz)_6][Ag(trz)_2]\}$ framework composed of the $[Ag_6(trz)_6]$ metallacycles (A), Ag4 and Ag6 ions (B) and linear $[Ag(trz)_2]$ subunits (C). More specifically, six Ag ions (Ag2, Ag3 and Ag5) linking with six trz molecules give rise to a hexanuclear $[Ag_6(trz)_6]$ metallacycle (A) *via* the route Ag2–trz-2–Ag3–trz-1–Ag5–trz-3–Ag2–trz-2–Ag3–trz-1–Ag5–trz-3 (Fig. 2a). Different from **1**, the hexanuclear metallacycle exhibits a small double crown-like shape due to the different plane of six trz molecules under the action of Ag5–N11 bond. Then subunits A are connected together through Ag4 and Ag6 ions forming the 2D $\{Ag_3[Ag_6(trz)_6]\}_n$ sheet (Fig. 2b). Finally, the 2D sheets are further extends to a 3D framework *via* the subunit C $[Ag(trz)_2]$ shown in Fig. 2c. Consequently, subunit A as eight-connected nodes and B and C as two-connected node, fabricate a new framework with $\{4^2\}\{8^2\}\{4^2\cdot8^{20}\cdot12^6\}$ topology (Fig. 2c below). Due to the tortuosity of subunit A, the 3D framework possess a larger void with dimensions of *ca.* 22.242 Å × 22.242 Å. Taking no account of organic ligands, PMo_{12} clusters link with Ag1, Ag3, Ag4 and Ag6 ions forming the 2D inorganic layer (Fig. 3a). Note that PMo_{12} clusters using eight

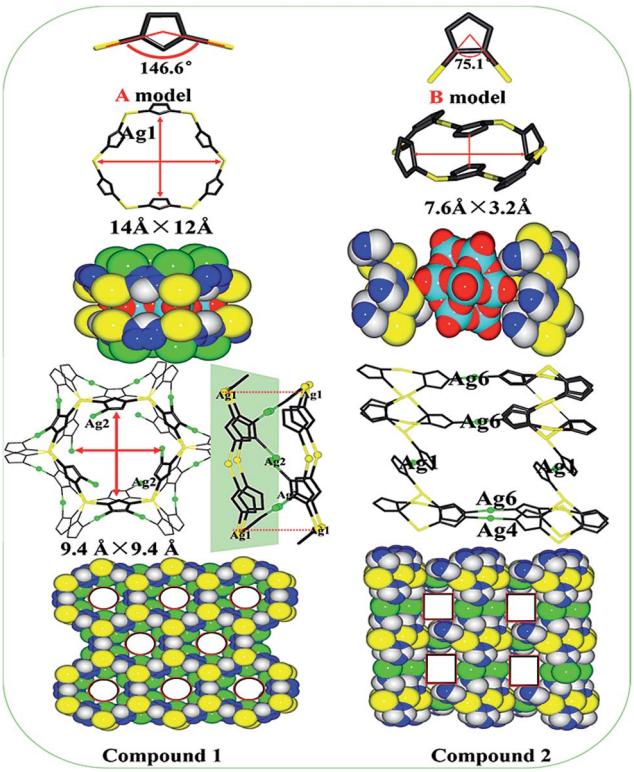

Scheme 1 Schematic view of the influence of the coordination modes of the trz ligand on the construction of metal–organic frameworks in compounds **1–2**.

terminal oxygen atoms coordinate with ten Ag^+ ions, which represents the highest terminal oxygen coordination number of Keggin POMs up to date. As a result, the 2D inorganic layer intersect with the 3D $\{Ag_3[Ag_6(trz)_6][Ag(trz)_2]\}$ framework by sharing ten Ag ions (two Ag1, two Ag3, two Ag4 and four Ag6) fabricating the whole structure, in which PMo_{12} clusters are located in the center of channels (Fig. 3b). From the topological view, compound **2** exhibits a unique (4, 4, 4, 10, 10)-connected 3D framework with an unprecedented $\{3\cdot4^3\cdot5\cdot6\}_2\{3^2\cdot4^2\cdot5^2\}\{3^2\cdot4^3\cdot5\}\{3^6\cdot4^{12}\cdot5^8\cdot6^{14}\cdot7^4\cdot8\}\{3^6\cdot4^{14}\cdot5^{10}\cdot6^{13}\cdot7\cdot8\}$ topology (Fig. 3d). In this simplification, the four-connected nodes are Ag1, Ag4 and Ag6, and ten-connected nodes are hexanuclear $[Ag_6(trz)_6]$ subunits and PMo_{12} clusters.

By the utilization of the same ingredients, two new silver–triazole frameworks with Keggin POMs templates have been fabricated and summarized shown in Scheme 1. It seems that the coordination modes of trz ligand (pyrazole-like 1,3-coordination (named as A) and imidazole-like 1,2-coordination (named as B)) and the template of PMo_{12} polyanions have an important influence on the structures of **1** and **2**. In **1**, each trz ligand coordinates with Ag ions forming a bigger twist angle (146.6°), which can reduce the interaction between adjacent atoms. Then the larger hexanuclear metallacycle $[Ag_6(trz)_6]$ with the dimension of 14 Å × 12 Å was successfully constructed, and the similar result was observed in compound $[Ag_6(trz)_6][PMo_{12}O_{40}]_2\cdot6H_2O$.[42] So the sphere PMo_{12} polyanions with the dimension of 10.4 Å × 10.4 Å can be easily located in the hexanuclear macrocycle. Meanwhile, the PMo_{12} clusters as templates induce the coordination between Ag2 and hexanuclear metallacycle, which results in a shrunken ten-nuclear metallacycle $[Ag_{10}(trz)_8]$ with the dimension of 9.4 Å × 9.4 Å due to the conversion through mirror symmetry of the adjacent hexanuclear metallacycle. As the results, PMo_{12} polyanions are sandwiched in the interior of the ten-nuclear metallacycle. Comparison with **1**, trz molecules coordinate with Ag ions forming a smaller twist angle (75.1°) in **2**, which increases the opportunities of the interaction among atoms, and the crown-like hexanuclear metallacycle with the dimension of 7.6 Å ×

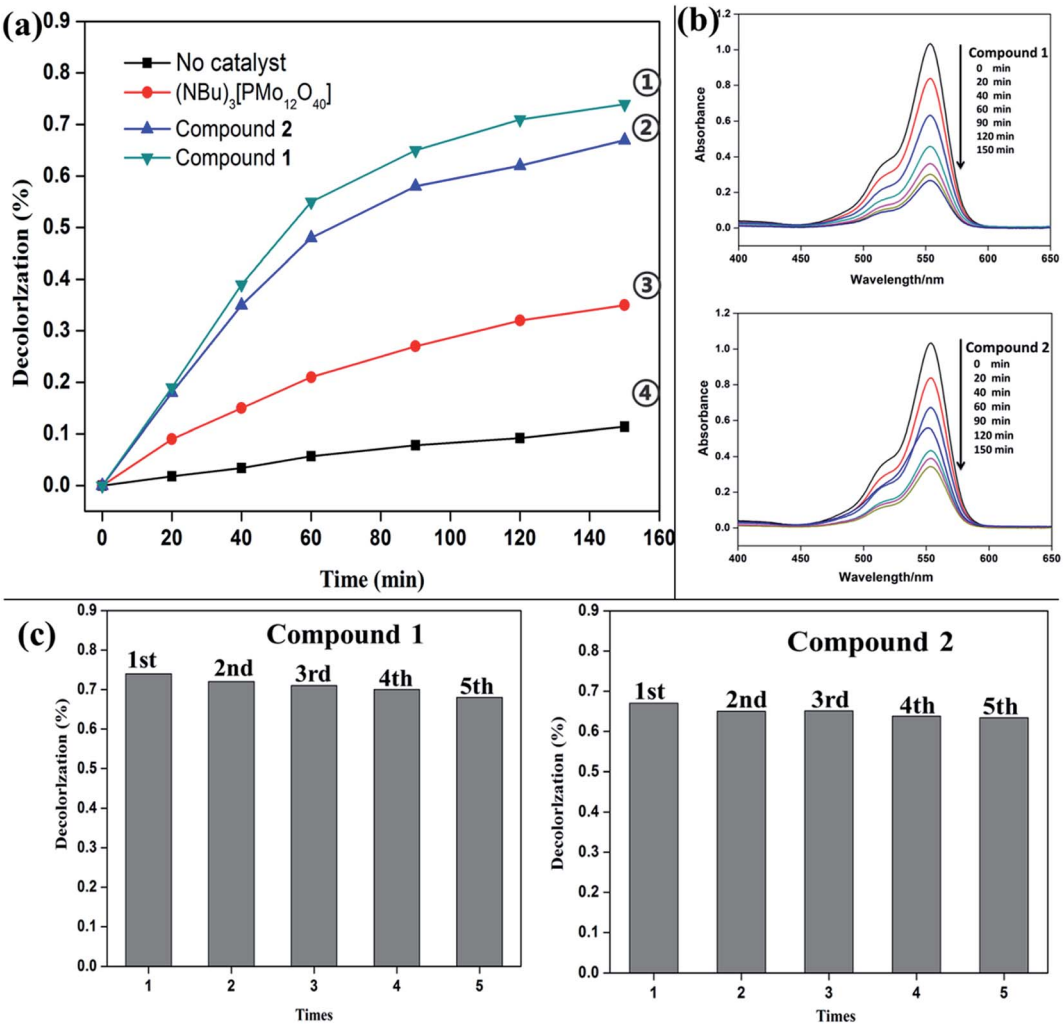

Fig. 4 (a) Decolorization of RhB solution in different reaction systems. Compound **1** as catalyst (①), compound **2** as catalyst (②), $(NBu)_3[PMo_{12}O_{40}]$ **1** as catalyst (③) and no catalyst (④) under UV irradiation. (b) UV-vis adsorption spectra of the RhB solution under UV irradiation in the presence of the compounds **1**–**2**. (c) Recycling experiments using compounds as catalyst for the photocatalytic degradation of RhB under UV irradiation.

3.2 Å is constructed (Ag2···Ag3 = 3.26 Å, Ag3···Ag5 = 3.19 Å). So the PMo_{12} polyanions with lager size (*ca.* 10.4 Å × 10.4 Å) were rejected outside the window of crown-like macrocycle as templates forming the open sandwich structure, which provides more space to coordinate with Ag ions (Ag1, Ag4 and Ag6). As a result, a 3D $\{Ag_3[Ag_6(trz)_6][Ag(trz)_2]\}$ framework with 2D channels with dimensions of *ca.* 22.242 Å × 22.242 Å are perfectly fabricated under the template of PMo_{12} polyanions, in which PMo_{12} polyanions locate in the center of channels.

XRD pattern, IR spectra and optical energy gap

The XRD patterns for **1** and **2** are presented in Fig. S5 (ESI†). The diffraction peaks of both simulated and experimental patterns match well, except for a little difference about reflection intensities, thus indicating that the new compounds are the purity phase. In addition, XRPD of **1** and **2** have exactly similarity of peak position and intensity before and after photo-degradation of RhB, which confirms the stability of compounds as photocatalyst. IR spectra of **1** and **2** are presented in Fig. S6 (ESI†). Characteristic peaks at 1057, 956, 887 and 796 cm^{-1} for compound **1**, and 1057, 967, 897 and 795 cm^{-1} for **2**, are assigned to ν_{as}(P–O), ν_{as}(O–Mo), ν_{as}(Mo–O_b–Mo) and ν_{as}(Mo–O_c–Mo) vibrations. Vibration peaks in the region of 140–1156 cm^{-1} are regarded as to that of trz molecules. The diffuse reflectivity of **1** and **2** was measured in order to determine the band gaps (E_g), which is defined as reverse extension point between energy axis and linear Kubelka–Munk absorption intensity.[43,44] As shown in Fig. S7 (ESI†), according to the corresponding absorption intensity, E_g values of **1** and **2** are assessed as 2.04 eV and 1.78 eV, respectively. The result indicates that **1** and **2** have semiconductor properties and can be used as potential photocatalyst.

Photocatalysis properties

POMs and their derivatives have been proven to be an excellent kind of green and cheap photocatalysts for the degradation of the organic dyes, because the ultraviolet light can induce POM to produce oxygen-to-metal charge transfer (OMCT), promoting electron from the highest occupied molecular orbital (HOMO) to the lowest unoccupied molecular orbital (LUMO).[45,46] Then the charge transfer excited state (POM*) with strong oxidizing properties can not only directly oxidize the target pollutant, but also react with water or other electron donors to generate an ·OH radical. Herein, by selecting RhB as a model organic dye, the photocatalytic performances of compounds **1** and **2** under UV irradiation were tested, and the decomposition rates of RhB solution were calculated by the following formula:

$$D = \frac{C_0 - C}{C_0} \times 100\% = \frac{A_0 - A}{A_0} \times 100\%$$

where D is decomposition rate, C_0, A_0 and C, A are the concentration and absorbency of RhB solution in absorption equilibrium before and irradiation, respectively.

As shown in Fig. 4a and b, after irradiation for 150 min, the photocatalytic decomposition rates are 73.9% for **1** and 67.1% for compound **2** as catalyst. In contrast, the photocatalytic decomposition rate is 35.2% using insoluble $(NBu_4)_3[PMo_{12}O_{40}]$ as catalyst and 10.2% without catalyst after 150 min UV light irradiation, which illustrates that the formation of hybrid compound could improve the photocatalytic performance of the $(NBu_4)_3[PMo_{12}O_{40}]$. According to the photocatalytical mechanism of POMs, the enhanced photocatalytic property can be deduced that the cleavage of the whole chromophore structure of RhB occurs preferentially over the surface of compounds **1** and **2**, meanwhile the Ag–trz framework acts as photosensitizer and promotes transition of electrons to POMs. The minor difference between **1** and **2** may be caused by the different Ag–trz frameworks (2D honeycomb net for **1** and 3D porous framework for **2**) and the coordination number of Keggin POM (12 for **1** and 8 for **2**), which can affect the transition of electrons to POMs.

Further studies show that **1** and **2** are very stable and easily removed from the mixture solution, and the catalytic activity for subsequent run falls but little changes shown in Fig. 4c (73.9% for **1**, and 67.1% for **2** for the first cycles, 72.1% for **1** and 65.2% for **2** for the second cycles, 71.2% for **1** and 65.1% for **2** for the third cycles, 70.0% for **1** and 63.8% for the fourth cycles, 67.9% for **1** and 63.4% for **2** for the fifth cycles). The result indicates that **1** and **2** possess better degradation activity and may be an excellent potential photocatalyst to decompose some organic dye.

Conclusions

In summary, two new Ag–trz hybrid compounds with $[PMo_{12}O_{40}]^{3-}$ templates have been successfully synthesized and structurally characterized. The cooperative assembly of the diverse coordination mode of 1,2,4-triazole and the template induction of the oxygen-rich Keggin POMs gave rise to two different Ag–trz framework, which results in two new POMs-based hybrid compounds. Also, compounds **1** and **2** are efficient molecular photocatalyst for the degradation of RhB. This work may supply a new strategy for constructing new framework by employing POMs as templates, and encourage us to further explore the other POM template framework.

Acknowledgements

This work was financially supported by NNSF (no. 21271089, 21371099 and 21471080), and New Century Excellent Talents Program in Heilongjiang Province (1253-NCET-022) and Talent Culturing Plan for Leading Disciplines of University in Shandong Province.

Notes and references

1 M. Eddaoudi, J. Kim, N. Rosi, D. Vodak, J. Wachter, M. O'Keeffe and O. M. Yaghi, *Science*, 2002, **295**, 469.
2 N. L. Rosi, J. Eckert, M. Eddaoudi, D. T. Vodak, J. Kim, M. O'Keeffe and O. M. Yaghi, *Science*, 2003, **300**, 1127.
3 D. Chen, W. Shen, S. Wu, C. Chen, X. Luo and L. Guo, *Nanoscale*, 2016, **8**, 7172.

4 M. Müller, S. Hermes, K. Kähler, M. W. van den Berg, M. Muhler and R. A. Fischer, *Chem. Mater.*, 2008, **20**, 4576.
5 L. He, Y. Liu, J. Liu, Y. Xiong, J. Zheng, Y. Liu and Z. Tang, *Angew. Chem., Int. Ed.*, 2013, **52**, 3741.
6 D. Farrusseng, S. Aguado and C. Pinel, *Angew. Chem., Int. Ed.*, 2009, **48**, 7502.
7 J. K. Lee, J. H. Lee, N. H. Ahn, K. H. Cho and S. B. Hong, *Chem. Sci.*, 2016, **7**, 5805.
8 N. Chang, Z. Y. Gu, H. F. Wang and X. P. Yan, *Anal. Chem.*, 2011, **83**, 7094.
9 R. B. Getman, Y. S. Bae, C. E. Wilmer and R. Q. Snurr, *Chem. Rev.*, 2012, **112**, 703.
10 A. K. Cheetham, G. Férey and T. Loiseau, *Angew. Chem., Int. Ed.*, 1999, **38**, 3268.
11 K. Yamamoto, Y. Sakata, Y. Nohara, Y. Takahashi and T. Tatsumi, *Science*, 2003, **300**, 470.
12 M. R. Sambrook, P. D. Beer, J. A. Wisner, R. L. Paul and A. R. Cowley, *J. Am. Chem. Soc.*, 2004, **126**, 15364.
13 R. Vilar, D. M. P. Mingos, A. J. P. White and D. J. Williams, *Angew. Chem., Int. Ed.*, 1998, **37**, 1258.
14 K. T. Holman, M. M. Halihan, S. S. Jurisson, J. L. Atwood, R. S. Burkhalter, A. R. Mitchell and J. W. Steed, *J. Am. Chem. Soc.*, 1996, **118**, 9567.
15 C. Inman, J. M. Knaust and S. W. Keller, *Chem. Commun.*, 2002, **2**, 156.
16 A. Müller, F. Peters, M. T. Pope and D. Gatteschi, *Chem. Rev.*, 1998, **98**, 239.
17 J. Y. Niu, X. Q. Zhang, D. H. Yang, J. W. Zhao, P. T. Ma, U. Kortz and J. P. Wang, *Chem.–Eur. J.*, 2012, **18**, 6759.
18 X. L. Wang, Z. H. Chang, H. Y. Lin, A. X. Tian, G. C. Liu, J. W. Zhang and D. N. Liu, *CrystEngComm*, 2015, **17**, 895.
19 D. Hagrman, P. J. Hagrman and J. Zubieta, *Angew. Chem., Int. Ed.*, 1999, **38**, 3165.
20 X. F. Kuang, X. Y. Wu, R. M. Yu, J. P. Donahue, J. S. Huang and C. Z. Lu, *Nat. Chem.*, 2010, **2**, 461.
21 X. F. Kuang, X. Y. Wu, J. Zhang and C. Z. Lu, *Chem. Commun.*, 2011, **47**, 4150.
22 G. Férey, C. Mellot-Draznieks, C. Serre, F. Millange, J. Dutour, S. Surblé and I. Margiolaki, *Science*, 2005, **309**, 2040.
23 J. Juan-Alcañiz, M. Goesten, A. Martinez-Joaristi, E. Stavitski, A. V. Petukhov, J. Gascon and F. Kapteijn, *Chem. Commun.*, 2011, **47**, 8578.
24 S. S. Y. Chui, S. M. F. Lo, J. P. H. Charmant, A. G. Orpen and I. D. Williams, *Science*, 1999, **283**, 1148.
25 C. Y. Sun, S. X. Liu, D. D. Liang, K. Z. Shao, Y. H. Ren and Z. M. Su, *J. Am. Chem. Soc.*, 2009, **131**, 1883.
26 J. W. Sun, P. F. Yan, G. H. An, J. Q. Sha, G. M. Li and G. Y. Yang, *Sci. Rep.*, 2016, **6**, DOI: 10.1038/srep25595.
27 S. B. Li, L. Zhang, K. P. O'Halloran, H. Ma and H. J. Pang, *Dalton Trans.*, 2015, **44**, 2062.
28 X. X. Qi, J. H. Lv, K. Yu, H. Zhang, Z. H. Su, L. Wang and B. B. Zhou, *RSC Adv.*, 2016, **6**, 72544.
29 J. Y. Niu, M. L. Wei, J. P. Wang and D. B. Dang, *Eur. J. Inorg. Chem.*, 2004, **1**, 160.
30 M. T. Li, J. Q. Sha, X. M. Zong, J. W. Sun and P. F. Yan, *Cryst. Growth Des.*, 2014, **14**, 2794.
31 X. Wang, A. X. Tian and X. L. Wang, *RSC Adv.*, 2015, **5**, 41155.
32 J. Q. Sha, M. T. Li, J. W. Sun, P. F. Yan, G. M. Li and L. Zhang, *Chem.–Asian J.*, 2013, **8**, 2252.
33 J. Q. Sha, L. Y. Liang, J. W. Sun, A. X. Tian, P. F. Yan, G. M. Li and C. Wang, *Cryst. Growth Des.*, 2012, **12**, 894.
34 A. Dolbecq, E. Dumas, C. R. Mayer and P. Mialane, *Chem. Rev.*, 2010, **110**, 6009.
35 D. Y. Du, J. S. Qin, S. L. Li, Z. M. Su and Y. Q. Lan, *Chem. Soc. Rev.*, 2014, **43**, 4615.
36 J. W. Sun, P. F. Yan, G. H. An, J. Q. Sha, C. Wang and G. M. Li, *Dalton Trans.*, 2016, **45**, 1657.
37 Q. G. Zhai, X. Y. Wu, S. M. Chen, Z. G. Zhao and C. Z. Lu, *Inorg. Chem.*, 2007, **46**, 5046.
38 R. Yu, X. F. Kuang, X. Y. Wu, C. Z. Lu and J. P. Donahue, *Coord. Chem. Rev.*, 2009, **253**, 2872.
39 G. M. Sheldrick, *SHELX-97, Program for Crystal Structure Refinement*, University of Göttingen, Germany, 1997.
40 I. D. Brown and D. Altermatt, *Acta Crystallogr., Sect. B: Struct. Sci.*, 1985, **41**, 244.
41 V. A. Blatov, A. P. Shevchenko and V. N. Serezhkin, *J. Appl. Crystallogr.*, 2000, **33**, 1193.
42 X. M. Chen, D. S. Wang, Q. Z. Luo and R. Wang, *Z. Naturforsch., B: J. Chem. Sci.*, 2008, **63**, 489.
43 J. I. Pankove, *Optical Processes in Semiconductors*, Prentice Hall, Englewood Cliffs, NJ, 1971.
44 W. M. Wesley and W. G. H. Harry, *Reflectance Spectroscopy*, Wiley, New York, 1966.
45 N. Mizuno and M. Misono, *Chem. Rev.*, 1998, **98**, 199.
46 S. Kim, J. Yeo and W. Choi, *Appl. Catal., B*, 2008, **84**, 148.